Lower Aβ-PET signal in white matter lesions relates to higher extracellular free water in mixed small vessel disease and Alzheimer's pathology

Authors: Julie Ottoy[1*], Miracle Ozzoude[1*], Katherine Zukotynski[1,2,3,4], Min Su Kang[5], Sabrina Adamo[1], Christopher Scott[1], Joel Ramirez[1], Walter Swardfager[6], Benjamin Lam[7], Aparna Bhan[1], Parisa Mojiri[1], Alex Kiss[8], Stephen Strother[9,10], Christian Bocti[11], Michael Borrie[12], Howard Chertkow[13], Richard Frayne[14], Robin Hsiung[15], Robert Jr. Laforce[16], Michael D. Noseworthy[17,2], Frank S. Prato[12], Demetrios J. Sahlas[18], Eric E. Smith[19], Phillip H. Kuo[20], Jordan A. Chad[9,10], Ofer Pasternak[21], Vesna Sossi[15], Alexander Thiel[13], Jean-Paul Soucy[5], Jean-Claude Tardif[22], Sandra E. Black[1,7,†], Maged Goubran[1,9,23,†], for the Medical Imaging Trials Network of Canada (MITNEC) and Alzheimer's Disease Neuroimaging Initiative[**]

Affiliations:

[1]LC Campbell Cognitive Neurology Unit, Hurvitz Brain Sciences Program, Sunnybrook Research Institute, University of Toronto, Toronto, ON, Canada
[2]Departments of Medicine and Radiology, McMaster University, Hamilton, ON, Canada
[3]Department of Medical Imaging, Schulich School of Medicine & Dentistry, Western University, London, ON, Canada
[4]Department of Radiology, University of British Columbia, Vancouver, BC, Canada
[5]Montreal Neurological Institute, McGill University, Montreal, QC, Canada
[6]Department of Pharmacology & Toxicology, University of Toronto, Toronto, ON, Canada
[7]Department of Medicine (Division of Neurology), University of Toronto, Toronto, ON, Canada
[8]Department of Research Design and Biostatistics, Sunnybrook Research Institute, University of Toronto, Toronto, ON, Canada
[9]Department of Medical Biophysics, University of Toronto, Toronto, ON, Canada
[10]The Rotman Research Institute Baycrest, University of Toronto, Toronto, ON, Canada
[11]Service de Neurologie, Département de Medicine, Université de Sherbrooke, Sherbrooke, QC, Canada
[12]Lawson Health Research Institute, Western University, London, ON, Canada
[13]Jewish General Hospital and Department of Neurology and Neurosurgery, McGill University, Montreal, QC, Canada
[14]Departments of Radiology and Clinical Neuroscience, Hotchkiss Brain Institute, University of Calgary, Calgary, AB, Canada
[15]Physics and Astronomy Department and DM Center for Brain Health, University of British Columbia, Vancouver, BC, Canada
[16]Clinique Interdisciplinaire de Mémoire, Département des Sciences Neurologiques, Université Laval, Québec, QC, Canada
[17]Department of Electrical and Computer Engineering, McMaster University, Hamilton, ON, Canada
[18]Department of Medicine, McMaster University, Hamilton, ON, Canada
[19]Hotchkiss Brain Institute, University of Calgary, Calgary, AB, Canada
[20]Department of Medical Imaging, Medicine, and Biomedical Engineering, University of Arizona, Tucson, AZ, USA
[21]Departments of Psychiatry and Radiology, Brigham and Women's Hospital, Harvard Medical School, Boston, USA
[22]Montreal Heart Institute, Université de Montréal, Montreal, QC, Canada
[23]Physical Sciences Platform, Sunnybrook Research Institute, Sunnybrook Health Sciences Centre, Toronto, ON, Canada

** co-first authors, † co-senior authors*

*** Data used in preparation of this article were obtained, in part, from the Alzheimer's Disease Neuroimaging Initiative (ADNI) database (adni.loni.usc.edu). As such, the investigators within the ADNI contributed to the*

design and implementation of ADNI and/or provided data but did not participate in analysis or writing of this report. A complete listing of ADNI investigators can be found at: http://adni.loni.usc.edu/wp-content/uploads/how_to_apply/ADNI_Acknowledgement_List.pdf

Corresponding author:

Maged Goubran, Ph.D.
maged.goubran@utoronto.ca
+1-416-480-6100 Ext. 85410 2075
2075 Bayview Avenue, M6 West RM 176
Toronto, Canada, M4N 3M5

Sandra E. Black, M.D. Ph.D.
sandra.black@sunnybrook.ca
+1-416-480-4551
2075 Bayview Avenue, Room A421
Toronto, Canada, M4N 3M5

Abstract

Background and Objectives: Positron emission tomography (PET) with amyloid-ligands recently gained interest for evaluating white matter (WM) pathology. Here, we investigated the neurobiological underpinnings of the amyloid-PET signal in the WM using free water (FW) diffusion MRI in a mixed cohort of small vessel disease (SVD) and Alzheimer's disease (AD) pathology.

Methods: We included data from two large cohort imaging studies, including MITNEC-C6 with moderate-to-severe white matter hyperintensity (WMH) burden and ADNI-2 with mild-to-moderate WMH burden, covering the spectrum of cognitively normal to dementia. Subjects underwent diffusion MRI, ^{18}F-AV45 amyloid-PET, and cognitive testing. We calculated WM diffusion metrics including fractional anisotropy (FA) and mean diffusivity (MD). In addition, we applied a bi-tensor diffusion MRI model that differentiates between extracellular (FW fraction) and tissue-specific (FW-adjusted FA) compartments of the WM. We tested associations of all diffusion metrics with ^{18}F-AV45 SUVR in regions of WMH vs. normal-appearing WM (NAWM), and with cognition. We further performed partial-least-square analysis to investigate how the diffusion metrics as well as age, sex, education, WMH volume, and cortical ^{18}F-AV45 SUVR covary with WM ^{18}F-AV45 SUVR.

Results: ^{18}F-AV45 SUVR was significantly lower in regions of WMH compared to NAWM (t=25.08, P<0.0001, n=115 subjects). Within WMH, lower ^{18}F-AV45 SUVR was associated with higher FW (β=-0.36±0.13, P=0.005) and lower FA (β=+0.24±0.12, P=0.046), but not with the tissue-specific metric FW-adjusted FA. Partial-least-square analysis further confirmed that FW had the most influence on ^{18}F-AV45 SUVR in regions of WMH. In contrast, FW-adjusted FA had more influence on ^{18}F-AV45 SUVR in NAWM. Last, correlation with cognitive impairment was higher for FW than FW-adjusted FA, both in regions of WMH (MMSE: β_{FW}=-0.40±0.13, P=0.003; $\beta_{FW\text{-adjusted FA}}$=0.14±0.09, P=0.11) and NAWM (MMSE: β_{FW}=-0.30±0.11, P=0.01; $\beta_{FW\text{-adjusted FA}}$=0.21±0.09, P=0.02).

Conclusion: In a cohort representative of the more common AD population, reduced amyloid-PET uptake in WM lesions may largely reflect the appearance of extracellular FW, while changes in NAWM may associate with tissue-specific damage. Ultimately, our findings may support FW and amyloid-PET as markers of WM abnormalities in SVD and AD.

Introduction

^{18}F-Florbetapir is one of the most commonly used PET ligands to detect and quantify amyloid-β (Aβ) burden in the cortex of Alzheimer's disease (AD) patients. Specifically, Aβ ligands are thought to target the cross beta-sheet structure of the insoluble Aβ fibrils [1]. In addition to targeting fibrils in the cortex, these ligands are lipophilic in nature and show high retention in the white matter (WM) [1–3]. It is hypothesised that this high WM uptake is due to a similar beta-sheet structure of myelin basic protein [4] and that microstructural damage or demyelination of WM tracts, previously observed in AD [5], results in reduced ligand binding [6]. However, others did not observe specific binding of the Aβ-ligand to WM tissue sections, for example in AD and brain injury cohorts [3,7], and attributed high WM retention to slow WM kinetics [3]. As such, the molecular basis of Aβ-ligand binding to WM remains poorly understood.

Diffusion MRI (dMRI) is a useful imaging modality to study WM microstructure *in-vivo* [8] and may help to better understand the binding dynamics of Aβ-ligands to WM [9,10]. In diffusion tensor imaging (DTI) modeling of dMRI data, fractional anisotropy (FA) reflects an ellipsoid shape of diffusivity within a given voxel. Higher FA values are thought to arise from higher diffusivity along one preferred direction (i.e., along intact myelinated fibers, thus representing fiber integrity) or from a loss of crossing fibers [11–13]. On the other hand, mean diffusivity (MD) represents the magnitude of diffusion (average of eigenvalues) regardless of the directionality. Prior studies have shown lower FA and higher MD in areas of WM degradation such as those frequently observed as white matter hyperintensities (WMH) on Fluid Attenuated Inversion Recovery (FLAIR) MRI [14]. In addition, some found a link between lower FA and lower Aβ-PET signal in the WM; thus supporting Aβ-PET as an early, complementary marker of cortical Aβ and WM microstructural damage (demyelination/axonal loss [9,15]). However, the latter may be an oversimplistic interpretation of the altered Aβ-PET signal in WM as single-tensor DTI metrics such as FA are contaminated by signals from both adjacent cerebrospinal fluid (CSF) and freely diffusing water in the extracellular space surrounding the WM fiber tracts [16,17]. As such, conventional DTI metrics can hardly differentiate between degenerative and vascular/neuroinflammatory changes underlying altered Aβ-PET uptake in the WM. This bias will be exemplified in subjects with pronounced atrophy, enlarged CSF spaces, and vasogenic

edema surrounding collagenosed venules; all of which are encountered in the more general AD population with co-existent small vessel disease (SVD) pathology [18,19].

Recently, a *bi*-tensor (two-compartment) model of dMRI was proposed to isolate the extracellular free water (FW) compartment from the tissue-specific (WM fibers) compartment within every image voxel [20,21]. In the human brain, FW is found as blood, interstitial fluid and CSF within ventricles and surrounding brain parenchyma, while it also accumulates as a form of edema in the extracellular spaces of structures distal from CSF such as deep WM [20]. Changes in FW may indicate extracellular processes including vascular damage and inflammation. On the other hand, changes in FW-adjusted DTI metrics (e.g., FW-adjusted FA) may be closer related to microstructural tissue damage and fiber integrity [20,22]. To our knowledge, no studies have yet investigated the link between Aβ-PET uptake in the WM and WM microstructure using multi-compartment diffusion modeling, specifically FW imaging. Furthermore, FW itself was recently proposed as a standalone biomarker of early vascular changes and cognitive impairment in AD, SVD, and mixed disease [21,23–26]. To this end, the primary aim of this study was to investigate the origin of the non-specific Aβ-PET signal in the WM using FW imaging. Such research may ultimately support Aβ-PET and FW as potential markers of WM abnormalities in AD and SVD.

Methods

Participants

The study included a total of 115 participants. Fifty-eight participants were recruited from dementia/stroke-prevention clinics as part of the multicenter C6 project of the Medical Imaging Network of Canada (MITNEC-C6) across seven participating sites. These participants showed moderate-to-severe SVD as quantified by Fazekas-score>2 and high (>10cm^3[27]) confluent periventricular WMH volumes [median(IQR): 31.09(22.36)cm^3]. Detailed selection criteria are described in [28,29] and summarized in **Supplementary Table 1**. Additionally, fifty-seven cognitively normal and mild cognitive impairment (MCI) participants were included from the Alzheimer's Disease Neuroimaging Initiative (ADNI-2) database with low-to-moderate WMH volumes [median(IQR): 5.84(9.17)cm^3]. General demographics included: age≥60y, education>8y, and MMSE≥20; see **Table 1** describing demographics for both groups (i.e., ADNI-2 and MITNEC-C6, further referred to as the *low* and *high* WMH group, respectively). Both groups were matched for vascular risk factors including hypertension, pulse pressure, BMI, sex, and smoking status [28]. All participants underwent Aβ-PET (^{18}F-AV45), 3T MRI including 3D T1, FLAIR, single-shell dMRI (detailed acquisition parameters, according to MRI scanner vendor, are provided in **Supplementary Table 2**), and a neuropsychological assessment.

Standard Protocol Approvals, Registrations, and Patient Consents

Image quality control, archiving of clinical and imaging data, and access to pipelines was performed at the Sunnybrook Research Institute through a common database. All participants provided written informed consent. The institutional review boards at all participating institutions approved this study.

Regarding ADNI data; ADNI was launched in 2003 as a public-private partnership. The primary goal of ADNI was to test whether MRI, PET, other biological markers, and clinical data can be combined to measure the progression of MCI/AD [see www.adni-info.org].

Neuropsychological assessment

Detailed neuropsychological assessments used for this study are previously described [28]. In brief, processing speed and executive function were measured with the Trail Making Test (Trails) parts A (n=115) and B (n=114). They were log-transformed to achieve a normal distribution. In addition, semantic fluency was measured with animal naming (n=115) and global cognition was measured with the Mini-Mental State Examination (MMSE, n=115).

Structural MRI

MRI was performed using acquisition protocols that were standardized across vendor platforms and compatible with the ADNI-2 protocol [30] (see **Supplementary Table 2)**. We used the same MRI processing methodology as the one employed in a previous study [28]. Briefly, the T1-weighted MRI images were processed using FreeSurfer v6.0 using an in-house modified pipeline for subjects with SVD [31]. Subcortical lacunar infarcts were masked out using the SABRE-Lesion Explorer pipeline before WMH segmentation [32]. WMH were delineated based on our automated segmentation tool 'HyperMapper' that uses T1, FLAIR, and Bayesian 3D Convolutional Neuronal Networks (CNN) [33]. Total WMH volume was normalized by the total intracranial volume (ICV), and log-transformed. Total ICV was estimated using a skull-stripping deep learning network developed in-house that is robust to vascular lesions and atrophy [34].

The NAWM was segmented in native space by subtracting the binarized WMH regions from the binarized whole WM defined by the Desikan-Killiany-Tourville (DKT) atlas of FreeSurfer. To limit partial volume effects, we 1) did not include ADNI subjects with very low WMH volume <1000mm^3 (no MITNEC-C6 subjects fulfilled this criteria), 2) used a more liberal HyperMapper threshold on segmentation probabilities (0.4-0.5) to avoid overestimation of WMH volumes [33], and 3) performed erosion on the NAWM masks by 2x2x2mm^3 to eliminate spill-in from neighboring tissue including cortex and CSF. **Figure 1** highlights WMH and NAWM delineations in an example subject.

Diffusion tensor imaging

The dMRI scans were acquired based on standardized acquisition protocols across vendor platforms and were compatible with the ADNI-2 protocol. In brief, ADNI data (corresponding to

our low WMH group) was downloaded from the ADNI-2 database. Acquisition parameters included 256×256 matrix size, 1.4×1.4×2.7mm^3 voxel size, 9000ms TR, and 9min dMRI scan time. A total of 41 diffusion encoding directions (b=1000s/mm^2) and five b=0s/mm^2 (T2-weighted images with no diffusion sensitization) were acquired. More details can be found in http://adni.loni.usc.edu/wp-content/uploads/2010/05/ADNI2_GE_3T_22.0_T2.pdf. In the MITNEC-C6 cohort (corresponding to our high WMH group), dMRI scans were acquired using a 128×128 matrix size, 2mm isotropic voxels, TR ranging between 9400 and 10000ms depending on the vendor, and 30 or 32 directions depending on the vendor with a b value=1000s/mm^2. Full acquisition protocols are included in **Supplementary Table 2.** The preprocessing steps to obtain corrected dMRI data and DTI scalar maps (FA and MD) are outlined in [35]. In brief, the dMRI data was corrected for susceptibility-induced field distortions and eddy current-induced distortions and motion correction using FSL [36]. Tensor fitting was conducted with a weighted-least square, generating DTI scalar metrics including FA and MD maps in T1 native space.

For FW mapping, the eddy current and motion-corrected dMRI data were fitted to a two-compartment diffusion model in each voxel, separating the FW compartment from the non-FW tissue compartment [20] (**Figure 2**). Specifically, an FW map represents the fractional volume (ranging from 0 to 1) of freely diffusing extracellular water with a fixed isotropic diffusivity of 3×10^{-3} mm^2/s (the diffusion coefficient of water at body temperature). The FW-corrected FA represents the FA signal following removal of the FW signal and is expected to be more specific to axonal and myelination changes than FA alone [16] (**Figure 2**). All DTI images were checked visually for quality assurance and scans with excessive motion and/or artifacts were excluded (n=5; not included in demographics nor analyses). Subsequently, the mean FA, MD, FW, and FW-adjusted FA were extracted in the whole brain (WB), WMH, and NAWM. As described in [20] the FW was scaled by the signal acquired for zero diffusion weightings, while FA, MD, and FW-adjusted FA were scaled by their respective WB values assuming site/scanner differences may affect the global metric [37,38]. **Figure 1** shows an example of a T1-weighted image with corresponding DTI-based scalar maps.

Amyloid-PET imaging

^{18}F-AV45 scans were acquired for all subjects as per the ADNI-2 imaging protocol [see http://adni.loni.usc.edu/wp-content/uploads/2008/07/adni2-proceduresmanual.pdf]. We used the same PET processing methodology as the one employed in a previous study [28]. Standardized uptake value ratios (SUVR) were generated in the WMH and NAWM masks and referenced to the cerebellum. A 'global' Aβ SUVR value was derived based on the AD-signature regions from Jack's mask (volume-weighted average of the frontal, parietal, temporal, and cingulate regions) [39]. 22.8% and 46.6% were considered Aβ-positive in our low and high WMH groups, respectively, based on a quantitative ^{18}F-AV45 SUVR cut-off of 1.1 in the AD-signature [28]. Mean SUVR values within WMH and NAWM were extracted for each subject in their T1 native space.

Statistical analyses

Statistics were performed using Python v3.7 and R v4.0. All continuous metrics were z-scored to allow for direct comparison between models across predictors and outcome measures. Values are reported as mean ± standard error (SE), unless stated otherwise. A two-tailed t-test for continuous variables and chi-square for categorical variables were used to detect significant differences in demographics between the low and high WMH groups.

1. Differences in ^{18}F-AV45 SUVR and DTI metrics between NAWM and WMH

A paired t-test was used to detect significant differences in ^{18}F-AV45 SUVR or DTI metrics between NAWM and WMH.

2. Regression between ^{18}F-AV45 SUVR and DTI metrics

Linear regressions were used to assess the associations between each of the DTI metrics (independent variable) and ^{18}F-AV45 SUVR (dependent variable) in NAWM or WMH, adjusted for continuous age and education, and sex. The regressions evaluated in the WMH were additionally adjusted for global cortical Aβ SUVR and for WMH volume, which was previously shown to be significantly associated with WMH ^{18}F-AV45 SUVR [40] and may additionally

account for inter-cohort differences in global WMH burden. The regressions evaluated in the NAWM were adjusted for global cortical Aβ SUVR to account for spill in from the cortex [9]; WMH volume was not significantly associated with NAWM ^{18}F-AV45 SUVR and thus omitted as covariate (P>0.05). All regressions included bootstrapping using 1,000 replications and 0.8 sample fraction, and they were evaluated across all subjects as well as within the high WMH group separately. We did not investigate regressions within the low WMH group separately due to the limited resolution associated with the PET signal in small WMH volumes.

3. *Partial least square (PLS) analyses*

PLS-regression analyses were performed to further investigate how the closely related DTI metrics, as well as demographical (age, sex, education) and imaging (WMH volume, cortical Aβ SUVR) variables, covary together in predicting ^{18}F-AV45 SUVR in the WMH or NAWM. The number of components was determined based on the root-mean square error derived from ten-fold cross-validation with five repeats.

4. Regression between DTI metrics and cognitive impairment

Lastly, linear regression analysis was employed to assess the associations between DTI metrics in WMH or NAWM (FW and FW-adjusted FA; independent variable) and cognitive scores (dependent variable), adjusted for age, sex, education, WMH volume, and global cortical Aβ SUVR. The regressions included bootstrapping using 1,000 replications and 0.8 sample fraction.

5. Linear mixed-effect models

To investigate the effects of age or sex on ^{18}F-AV45 SUVR in the WM, we employed linear mixed effect models with an interaction term between age or sex and WM region (NAWM and WMH) and subject as a random factor.

Data and materials availability

All data associated with this study are available in the main text or the supplementary materials. All the imaging data will be shared upon request with a proposal and under a data transfer agreement.

Results

1. ^{18}F-AV45 SUVR and DTI metrics are altered in WMH compared to NAWM

Regions of WMH showed significantly lower ^{18}F-AV45 SUVR compared to NAWM (t=25.08, P<0.0001) (**Figure 3** left). In addition, regions of WMH showed significantly higher FW (t=-27.11, P<0.0001) and lower FW-adjusted FA (t=12.26, P<0.0001) compared to NAWM (**Figure 3** middle, right). Lastly, regions of WMH showed significantly higher MD (t=-24.37, P<0.0001) and lower FA (t=32.77; P<0.0001) compared to NAWM.

FW correlated strongly (Pearson's r > 0.5) with both FA and MD in WMH and with FA in NAWM, but not with FW-adjusted FA indicating that the FW effect was indeed removed from FW-adjusted FA (**Supplementary Figure 1**).

2. Lower ^{18}F-AV45 SUVR relates to higher FW in WMH and to higher FW-adjusted FA in NAWM

In regions of WMH, lower ^{18}F-AV45 SUVR was strongly associated with higher FW both across all subjects (β=-0.36±0.13, P=0.005; 95%$CI_{bootstrap}$[-0.50,-0.23]) (**Figure 4**A) and in the high WMH group separately (β=-0.33±0.14, P=0.019; 95%$CI_{bootstrap}$ [-0.46,-0.20]); results were not separately investigated in the low WMH group (cf. Methods section). In addition, lower ^{18}F-AV45 SUVR in regions of WMH was associated with higher FA (β=+0.24±0.12, P=0.046; 95%$CI_{bootstrap}$ [+0.12,+0.36]) across all subjects, but not with the tissue-specific metric FW-adjusted FA. Last, we found a trend towards an inverse association with MD across all subjects (P=0.064).

In the NAWM, ^{18}F-AV45 SUVR was inversely associated with FW-adjusted FA in the high WMH group (β=-0.32±0.12, P=0.008; 95%$CI_{bootstrap}$ [-0.43,-0.19]) and showed a trend across all subjects (P=0.077). In addition, there was a trend towards an association with FW

across all subjects (P=0.059; **Figure 4**B), while no associations were found with MD or FA in the NAWM.

In the PLS analysis of diffusion metrics, imaging variables (WMH volume and cortical ^{18}F-AV45 SUVR) and demographic variables (age, sex, and education), the first and second components explained 24% and 2%, respectively, of the variance of ^{18}F-AV45 SUVR in WMH (**Figure 5**A; high WMH group). Here, FW and WMH volume loaded most strongly inversely onto the first component, while FW-adjusted FA also had a significant but smaller contribution. This may indicate that lower ^{18}F-AV45 SUVR in regions of WMH is associated with both higher FW and WMH volume but to a lesser extent with FW-adjusted FA.

In NAWM, the first component explained 31% of the variance in ^{18}F-AV45 SUVR (**Figure 5**B; high WMH group). Here, cortical Aβ SUVR loaded most strongly positively onto this component, while FW-adjusted FA loaded significantly in an inverse way. This may indicate that higher ^{18}F-AV45 SUVR in NAWM is associated with higher cortical Aβ together with lower FW-adjusted FA.

Similar results were found across all subjects, except that FW-adjusted FA did not contribute to the first components (**Supplementary Figure 2**).

3. Increased FW in WM is associated with cognitive impairment

In regions of WMH, higher FW was associated with lower MMSE and semantic fluency both across all subjects (**Figure 6**A) and in the high WMH group separately (**Supplementary Table 3**). In addition, significant associations were found with processing speed and executive function for all subjects combined (**Supplementary Table 3**). Interestingly, lower ^{18}F-AV45 SUVR in regions of WMH was associated (P=0.016) with impaired executive function across all subjects after adjusting for WMH volume and cortical Aβ SUVR, but not (P=0.083) after additionally adjusting for FW.

Similarly, in the NAWM, higher FW was associated with lower MMSE and semantic fluency both across all subjects (**Figure 6**B) and in the high WMH group separately (**Supplementary Table 4**). In addition, significant associations were found with processing speed and executive function for all subjects (**Supplementary Table 4**). FW-adjusted FA in the

NAWM was significantly associated only with MMSE across all subjects (β=0.21±0.09, P=0.02; 95%$CI_{bootstrap}$ [0.10,0.31]).

4. Effects of age and sex on ^{18}F-AV45 SUVR in the WM

We found a significant interaction effect (P<0.0001) between age and WM region (i.e., NAWM vs WMH) on ^{18}F-AV45 SUVR, such that older age was associated with lower ^{18}F-AV45 SUVR in the WMH but with higher ^{18}F-AV45 SUVR in the NAWM (**Supplementary Figure 3**). However, when this model was evaluated within the NAWM and WMH separately, no significant associations between age and WM ^{18}F-AV45 SUVR were found. No interactive effect was found between sex and WM region on ^{18}F-AV45 SUVR. However, females showed consistently higher ^{18}F-AV45 SUVR in both NAWM (P=0.008) and WMH (P=0.006) compared to males (**Supplementary Figure 4**).

Discussion

This study investigated the neurobiological underpinnings of Aβ-PET (^{18}F-AV45) uptake in the WM using two-compartment modelling of dMRI in a mixed cohort spanning mild to severe WMH burden and AD pathology. Our main findings were: 1) In regions of WMH, lower ^{18}F-AV45 PET was most strongly associated with higher FW; 2) In NAWM, lower ^{18}F-AV45 PET was most strongly associated with lower cortical Aβ and higher FW-adjusted FA; and 3) higher FW in both regions of WMH and NAWM was associated with cognitive impairment. These findings have three main implications: 1) Lower ^{18}F-AV45 PET in WMH may reflect vascular damage, edema, inflammation, and/or necrosis, which should be accounted for when normalizing cortical Aβ SUVR with a WM reference region in subjects with vascular co-pathology [20]; 2) lower ^{18}F-AV45 PET in NAWM may track with cortical Aβ and partly reflect fiber-specific damage, and 3) FW may be considered as a sensitive SVD biomarker in AD to detect early and more subtle changes in WM microstructure [21,23].

Akin to studies in demyelinating diseases such as multiple sclerosis (MS) [41–43], studies in cognitively normal and AD showed lower Aβ-PET uptake in areas of damaged WM [9,10,15,44], suggesting Aβ-PET as a biomarker of demyelination. Specifically, they postulated that binding of the Aβ-ligand occurs in between intact myelin sheets and that the uptake of the PET signal is

reduced due to loss of the myelin fibers. This was demonstrated for the first time by Stankoff et al. [6] in primates and two MS patients where ^{11}C-PiB PET was well associated with PiB staining of myelin. Several other groups subsequently studied Aβ-ligand retention in relation to *in-vivo* structural imaging techniques such as DTI and found lower FA and higher MD in regions of WM degradation, suggesting Aβ-PET as a biomarker of myelin integrity and axonal loss [9,15]. However, these studies did not account for contributions of FW to FA, ultimately limiting its interpretation and potentially overestimating the level of demyelination or axonal damage [17].

While we confirm prior studies by reporting a positive association between ^{18}F-AV45 PET and FA in regions of WMH (before FW adjustment) [9], we notably showed that ^{18}F-AV45 PET was more strongly associated with FW than with either FA or FW-adjusted FA in regions of WMH. This may indicate that the PET signal within imaging-visible WM lesions is more profoundly associated with changes in the extracellular space (potentially of vascular or inflammatory origin and/or reflecting extreme tissue loss and necrosis [20]) than with fiber-specific degradation. There are several additional considerations potentially supporting this theory. First, while demyelination may be an early feature in AD [5], its origin and/or interactions with the Aβ-ligand may depend on the degree of WM degradation (e.g., WMH vs. NAWM) as well as the underlying pathology (for instance, demyelination is the dominant feature in MS). Second, to our knowledge, no autofluorescence-based studies to date showed a direct link between myelin loss and ^{18}F-AV45 PET signal. Third, several studies reported a lack of specific PiB binding to WM tracts in brain sections of normal controls [3] or patients with traumatic brain injury [7] and AD [3]. In fact, a study by De Paula Faria et al. [45] showed that an Aβ-ligand (^{11}C-PiB) was the least favorable among three ligands to detect demyelinated and remyelinated lesions in a rat model of MS. Taken together, we speculate that reduced ^{18}F-AV45 retention in WM lesions is at least partly reflective of increased water content in mixed AD and SVD. The physiological mechanisms underlying FW increases in the WM remain unknown; they may be the result of a mixed pathological state involving edema, neuroinflammation, reduced cell density, blood brain barrier (BBB) leakage, ischemia, and ultimately damage to myelin membranes and the formation of visible WMH [46–48]. The presence of imaging-visible WMH is known to be associated with an increased risk of cognitive decline and dementia [49].

^{18}F-AV45 SUVR was on average 14% lower in regions of WMH compared to NAWM across all subjects, similar to prior reports [41]. A potential explanation for reduced Aβ-PET signal

in regions of the WMH may be alterations in the blood-brain-barrier permeability and the ligand's pharmacokinetics involving slower delivery rate to and/or faster washout from WM lesions (e.g., it may take longer for the ligand to reach a transient equilibrium state in WMH compared to NAWM [3,50]). Prior work with ^{18}F-AV45 has shown that 20% reduction in WM blood flow was associated with less than 5% reduction in SUVR at 50-60min post-injection [51]; as such, we do not believe that that the ~15% reduction in WMH ^{18}F-AV45 SUVR would be fully attributable to changes in blood flow. Alternatively, reduced ^{18}F-AV45 PET may simply reflect dilution of the signal due to extensive water accumulation surrounding the tissue. Nonetheless, altered ^{18}F-AV45 PET signal in WM lesions affects the use of WM as a reference region to quantify cortical Aβ SUVR in subjects with considerable WMH burden. Future studies should compare WM SUV between diagnostic groups [2] and either mask out WMH from the WM reference region and/or use WMH volume as a covariate in the analyses. In addition, other factors such as sex and age should be considered when using WM as a reference region. We and others [9] detected a differential effect of age on ^{18}F-AV45 SUVR in the NAWM vs. WMH. Specifically, the increase in NAWM ^{18}F-AV45 SUVR with aging seemed to be attenuated in WMH, indicating that older subjects with high WMH burden may show relatively lower ^{18}F-AV45 SUVR in the whole WM. Apart from an aging effect, we also found that females showed higher WM ^{18}F-AV45 SUVR compared to males.

In NAWM, lower FW-adjusted FA did not translate into lower ^{18}F-AV45 SUVR in our study. Instead, we demonstrated that lower FW-adjusted FA in the NAWM was associated with *higher* ^{18}F-AV45 SUVR both in the NAWM and in the cortex. This may indicate that subjects with high cortical Aβ load show more structural damage (~lower FW-adjusted FA) in their NAWM [52] but that this focal damage in the NAWM is not reflected by reduced Aβ-ligand uptake in the *whole* NAWM [9]. Previous research similarly indicated that the non-specific (off-target) WM PET signal is positively correlated with cortical PET signal even after partial volume correction/erosion [9,53]. It has been hypothesized that this WM-cortex PET correlation may be partly due to an additive off-target signal within the cortex, which may explain the improved stability of longitudinal PET in AD target regions using white matter as a reference region [53]. Apart from the WM-cortex correlation in PET signal, the relationship between lower ^{18}F-AV45 SUVR and higher FW-adjusted FA may also be explained by a loss of crossing fibers typically resulting in higher FA and FW-adjusted FA [11,13,54]. For example, Douaud et al.[12] showed that the

only region where DTI metrics were significantly different between healthy controls and MCI was an area of crossing fibers in the centrum semiovale; here, the motor-related projection fibers that crossed the degenerating fibers were selectively preserved, resulting in an increased FA in MCI. Our future work using tractography will investigate whether the inverse relationship between ^{18}F-AV45 SUVR and FW-adjusted FA in NAWM is related to crossing fibers.

Importantly, although lower FW-adjusted FA did not translate into lower ^{18}F-AV45 SUVR signal in the whole NAWM, we found a reduction of ^{18}F-AV45 SUVR in the NAWM in subjects with >30cc WMH volumes (**Supplementary Figure 5**). This may be due to microstructural changes (altered FW and/or FW-adjusted FA) spreading beyond the visible damage of the WMH into the surrounding penumbras of WMH, NAWM and connected tracts [15,55–57], potentially through Wallerian-type degeneration [58] or as part of the same continuum of microstructural damage. Indeed, our study indicated increases of FW in NAWM and associations with MMSE, potentially reflecting mild vascular damage in the NAWM and an early, pre-lesional role for FW in affecting cognitive function. Similarly, Ji et al. [21] found that AD subjects with and without concomitant cerebrovascular disease had higher FW in their NAWM compared to control subjects and that this higher level of FW contributed to the symptom severity. Apart from the FW-cognition relationship in NAWM, we found a similar and even stronger FW-cognition relationship within the WMH, underscoring FW as a potential WM disease-related biomarker in AD and SVD [21,24,26]. In fact, Maillard et al. [23] found that FW fully mediated the effect of WMH volume on cognition among older adults, while they reported a lack of association between FW-adjusted FA and cognition. Taken together, our findings emphasize the importance of quantifying WM changes in the early stages of the disease. In addition, eliminating or preventing excessive FW in the WM may serve as a potential preventive strategy (e.g., through earlier, more personalized vascular risk control) against vascular injury, cognitive decline, and progression to AD dementia.

Limitations of our study include the use of single-shell dMRI data and not accounting for crossing fibers nor the effects of capillary blood flow in the FW estimation. To estimate these factors, more diffusion encoding shells and directions, and arterial spin labeling (ASL) for microvascular perfusion estimation should be employed. Second, we focused on the averaged PET and DTI metrics within the NAWM and WMH. Thus, we cannot exclude that the FW-adjusted tissue compartment had more regional-specific associations with Aβ-PET and cognitive

performance [21]. Last, our study did not involve longitudinal data, which prevented us from inferring causality between WM microstructural changes (FW or FW-adjusted FA) and the Aβ-PET signal. The main strength of our study is the inclusion of normal elderly and real-world patients from dementia/stroke-prevention clinics covering the spectrum of low to severe WMH burden and AD pathology. In addition, by leveraging a novel DTI technique that adjusts FA for FW contributions, we provided novel insights into the relationship of WM microstructure with the non-specific ^{18}F-AV45 signal in the WM.

In conclusion, this study investigated the neurobiological underpinnings of Aβ-PET (^{18}F-AV45) uptake in the WM using dMRI. We found that lower Aβ-PET uptake in WM lesions is strongly linked to elevated FW, potentially reflecting vascular damage, edema, or inflammation. On the other hand, in the NAWM, the Aβ-PET uptake was more strongly associated with FW-adjusted FA. Last, in relation to cognition, higher FW both in WM lesions and NAWM related more closely to cognitive impairment than FW-adjusted FA. Our study may ultimately support the use of FW and Aβ-PET as potential biomarkers to detect WM abnormalities in AD and SVD.

Author contributions: JO and MO drafted the manuscript, participated in study concept and design, analyzed and interpreted the data. MG, SEB, and MSK revised the manuscript, participated in study concept and design, analyzed and interpreted data. KZ, PHK, SA, CS, JR, AP, PM, and BL contributed to data generation and revision. JAC and OP contributed to toolbox development and revised the manuscript. AK, SS, CB, MB, HC, RF, RH, RJL, MDN, FSP, DJS, EES, VS, AT, JPS, and JCT participated in study concept and design as site-leaders and revised the manuscript.

Acknowledgements: We would like to express our deepest gratitude towards all the participants and caregivers for their support and participation in this study. We are grateful to Eli Lilly & Company for providing the ^{18}F-florbetapir ligand. Our research was conducted with the support of the Ontario Brain Institute, an independent non-profit corporation, funded partially by the Ontario government. The opinions, results and conclusions are those of the authors and no endorsement by the Ontario Brain Institute is intended or should be inferred. In addition, part of the data collection and sharing for this project was funded by ADNI (National Institutes of Health Grant U01 AG024904) and DOD ADNI (Department of Defense award number W81XWH-12-2-0012). ADNI is funded by the National Institute on Aging, the National Institute of Biomedical Imaging and Bioengineering, and through generous contributions from the following: AbbVie, Alzheimer's Association; Alzheimer's Drug Discovery Foundation; Araclon Biotech; BioClinica, Inc.; Biogen; Bristol-Myers Squibb Company; CereSpir, Inc.; Cogstate; Eisai Inc.; Elan Pharmaceuticals, Inc.; Eli Lilly and Company; EuroImmun; F. Hoffmann-La Roche Ltd and its affiliated company Genentech, Inc.; Fujirebio; GE Healthcare; IXICO Ltd.; Janssen Alzheimer Immunotherapy Research & Development, LLC.; Johnson & Johnson Pharmaceutical Research & Development LLC.; Lumosity; Lundbeck; Merck & Co., Inc.; Meso Scale Diagnostics, LLC.; NeuroRx Research; Neurotrack Technologies; Novartis Pharmaceuticals Corporation; Pfizer Inc.; Piramal Imaging; Servier; Takeda Pharmaceutical Company; and Transition Therapeutics. The Canadian Institutes of Health Research is providing funds to support ADNI clinical sites in Canada. Private sector contributions are facilitated by the Foundation for the National Institutes of Health (www.fnih.org). The grantee organization is the Northern California Institute for Research and Education, and the study is coordinated by the

Alzheimer's Therapeutic Research Institute at the University of Southern California. ADNI data are disseminated by the Laboratory for Neuro Imaging at the University of Southern California.

Funding

This study was funded by the Canadian Institute for Health Research (CIHR) MOP Grant #13129, CIHR Foundation grant #159910, Ontario Brain Institute and the L.C Campbell Foundation. The work was also supported by the Medical Imaging Trial Network of Canada (MITNEC) Grant #NCT02330510. Matching funds were provided by participant hospital and research foundations, including the Baycrest Foundation, Bruyere Research Institute, Centre for Addiction and Mental Health Foundation, London Health Sciences Foundation, McMaster University Faculty of Health Sciences, Ottawa Brain and Mind Research Institute, Queen's University Faculty of Health Sciences, St. Michael's Hospital, Sunnybrook Health Sciences Centre Foundation, the Thunder Bay Regional Health Sciences Centre, University Health Network, the University of Ottawa Faculty of Medicine, and the Windsor/Essex County ALS Association. The Temerty Family Foundation provided the major infrastructure matching funds. JO is supported by the Alzheimer's Association fellowship (AARF-21-848556). MG is supported by the Donald Stuss Young Investigator innovation award and the Gerald Heffernan foundation.

References

1. Choi SR, Golding G, Zhuang Z, et al. Preclinical Properties of ^{18}F-AV-45: A PET Agent for Aβ Plaques in the Brain. J Nucl Med. 2009;50:1887–1894.

2. Ottoy J, Verhaeghe J, Niemantsverdriet E, et al. Validation of the Semiquantitative Static SUVR Method for ^{18}F-AV45 PET by Pharmacokinetic Modeling with an Arterial Input Function. J Nucl Med. 2017;58:1483–1489.

3. Fodero-Tavoletti MT, Rowe CC, McLean CA, et al. Characterization of PiB binding to white matter in Alzheimer disease and other dementias. J Nucl Med. 2009;50:198–204.

4. Harauz G, Ishiyama N, Hill CMD, Bates IR, Libich DS, Farès C. Myelin basic protein—diverse conformational states of an intrinsically unstructured protein and its roles in myelin assembly and multiple sclerosis. Micron. 2004;35:503–542.

5. Dean DC III, Hurley SA, Kecskemeti SR, et al. Association of Amyloid Pathology With Myelin Alteration in Preclinical Alzheimer Disease. JAMA Neurology. 2017;74:41–49.

6. Stankoff B, Freeman L, Aigrot M-S, et al. Imaging central nervous system myelin by positron emission tomography in multiple sclerosis using [methyl-11C]-2-(4′-methylaminophenyl)- 6-hydroxybenzothiazole. Ann Neurol. 2011;69:673–680.

7. Hong YT, Veenith T, Dewar D, et al. Amyloid Imaging With Carbon 11–Labeled Pittsburgh Compound B for Traumatic Brain Injury. JAMA Neurol. 2014;71:23.

8. Concha L. A macroscopic view of microstructure: Using diffusion-weighted images to infer damage, repair, and plasticity of white matter. Neuroscience. 2014;276:14–28.

9. Zeydan B, Schwarz CG, Lowe VJ, et al. Investigation of white matter PiB uptake as a marker of white matter integrity. Ann Clin Transl Neurol. 2019;6:678–688.

10. Goodheart AE, Tamburo E, Minhas D, et al. Reduced binding of Pittsburgh Compound-B in areas of white matter hyperintensities. Neuroimage Clin. 2015;9:479–483.

11. Teipel SJ, Grothe MJ, Filippi M, et al. Fractional Anisotropy Changes in Alzheimer's Disease Depend on the Underlying Fiber Tract Architecture: A Multiparametric DTI Study using Joint Independent Component Analysis. Journal of Alzheimer's Disease. IOS Press; 2014;41:69–83.

12. Douaud G, Jbabdi S, Behrens TEJ, et al. DTI measures in crossing-fibre areas: Increased diffusion anisotropy reveals early white matter alteration in MCI and mild Alzheimer's disease. NeuroImage. 2011;55:880–890.

13. Bergamino M, Walsh RR, Stokes AM. Free-water diffusion tensor imaging improves the accuracy and sensitivity of white matter analysis in Alzheimer's disease. Sci Rep. 2021;11:6990.

14. Maniega SM, Valdés Hernández MC, Clayden JD, et al. White matter hyperintensities and normal-appearing white matter integrity in the aging brain. Neurobiol Aging. 2015;36:909–918.

15. Moscoso A, Silva-Rodríguez J, Aldrey JM, et al. 18F-Florbetapir PET as a marker of myelin integrity across the Alzheimer's disease spectrum. Eur J Nucl Med Mol Imaging [online serial]. Epub 2021 Sep 28. Accessed at: https://link.springer.com/10.1007/s00259-021-05493-y.

16. Metzler-Baddeley C, O'Sullivan MJ, Bells S, Pasternak O, Jones DK. How and how not to correct for CSF-contamination in diffusion MRI. NeuroImage. 2012;59:1394–1403.

17. Berlot R, Metzler-Baddeley C, Jones DK, O'Sullivan MJ. CSF contamination contributes to apparent microstructural alterations in mild cognitive impairment. NeuroImage. 2014;92:27–35.

18. Toledo JB, Arnold SE, Raible K, et al. Contribution of cerebrovascular disease in autopsy confirmed neurodegenerative disease cases in the National Alzheimer's Coordinating Centre. Brain. 2013;136:2697–2706.

19. Keith J, Gao F-Q, Noor R, et al. Collagenosis of the Deep Medullary Veins: An Underrecognized Pathologic Correlate of White Matter Hyperintensities and Periventricular Infarction? J Neuropathol Exp Neurol. 2017;76:299–312.

20. Pasternak O, Sochen N, Gur Y, Intrator N, Assaf Y. Free water elimination and mapping from diffusion MRI. Magnetic Resonance in Medicine. 2009;62:717–730.

21. Ji F, Pasternak O, Liu S, et al. Distinct white matter microstructural abnormalities and extracellular water increases relate to cognitive impairment in Alzheimer's disease with and without cerebrovascular disease. Alz Res Therapy. 2017;9:63.

22. Albi A, Pasternak O, Minati L, et al. Free Water Elimination Improves Test–Retest Reproducibility of Diffusion Tensor Imaging Indices in the Brain: A Longitudinal Multisite Study of Healthy Elderly Subjects. HUman Brain Mapping. 2016;0:1–15.

23. Maillard P, Fletcher E, Singh B, et al. Cerebral white matter free water: A sensitive biomarker of cognition and function. Neurology. 2019;92:e2221–e2231.

24. Duering M, Finsterwalder S, Baykara E, et al. Free water determines diffusion alterations and clinical status in cerebral small vessel disease. Alzheimers Dement. 2018;14:764–774.

25. Dumont M, Roy M, Jodoin P-M, et al. Free Water in White Matter Differentiates MCI and AD From Control Subjects. Front Aging Neurosci. 2019;11:270.

26. Huang P, Zhang R, Jiaerken Y, et al. White Matter Free Water is a Composite Marker of Cerebral Small Vessel Degeneration. Transl Stroke Res. Epub 2021 Feb 25.

27. DeCarli C, Murphy DGM, Tranh M, et al. The effect of white matter hyperintensity volume on brain structure, cognitive performance, and cerebral metabolism of glucose in 51 healthy adults. Neurology. 1995;45:2077–2084.

28. Ottoy J, Ozzoude M, Zukotynski K, et al. The interplay between vascular burden and cognition: Mediating roles of neurodegeneration and amyloid-PET in a mixed cohort of small vessel disease and Alzheimer's pathology. MedRxiv 2021 online publication.

29. Zukotynski K, Gaudet V, Kuo PH, et al. The Use of Random Forests to Classify Amyloid Brain PET. Clin Nucl Med. 2019;44:784–788.

30. Duchesne S, Chouinard I, Potvin O, et al. The Canadian Dementia Imaging Protocol: Harmonizing National Cohorts. Journal of Magnetic Resonance Imaging. 2019;49:456–465.

31. Ozzoude M, Ramirez J, Raamana PR, et al. Cortical Thickness Estimation in Individuals With Cerebral Small Vessel Disease, Focal Atrophy, and Chronic Stroke Lesions. Frontiers in Neuroscience. 2020;14:1330.

32. Ramirez J, Scott CJM, McNeely AA, et al. Lesion Explorer: A Video-guided, Standardized Protocol for Accurate and Reliable MRI-derived Volumetrics in Alzheimer's Disease and Normal Elderly. JoVE. Epub 2014 Apr 14.:50887.

33. Forooshani PM, Biparva M, Ntiri EE, et al. Deep Bayesian networks for uncertainty estimation and adversarial resistance of white matter hyperintensity segmentation [online]. Neuroscience; 2021 Aug. Accessed at: http://biorxiv.org/lookup/doi/10.1101/2021.08.18.456666. Accessed September 22, 2021.

34. Ntiri EE, Holmes MF, Forooshani PM, et al. Improved Segmentation of the Intracranial and Ventricular Volumes in Populations with Cerebrovascular Lesions and Atrophy Using 3D CNNs. Neuroinform. 2021;19:597–618.

35. Nir TM, Jahanshad N, Villalon-Reina JE, et al. Effectiveness of regional DTI measures in distinguishing Alzheimer's disease, MCI, and normal aging. NeuroImage: Clinical. 2013;3:180–195.

36. Haddad SMH, Scott CJM, Ozzoude M, et al. Comparison of quality control methods for automated diffusion tensor imaging analysis pipelines. Yap P-T, editor. PLoS ONE. 2019;14:e0226715.

37. Archer DB, Vaillancourt DE, Coombes SA. A Template and Probabilistic Atlas of the Human Sensorimotor Tracts using Diffusion MRI. Cerebral Cortex. 2018;28:1685–1699.

38. Cohen AH, Wang R, Wilkinson M, MacDonald P, Lim AR, Takahashi E. Development of human white matter fiber pathways: From newborn to adult ages. Int j dev neurosci. 2016;50:26–38.

39. Jack CR, Lowe VJ, Senjem ML, et al. 11C PiB and structural MRI provide complementary information in imaging of Alzheimer's disease and amnestic mild cognitive impairment. Brain. 2008;131:665–680.

40. Wang M-L, Yu M-M, Li W-B, Li Y-H. Longitudinal Association between White Matter Hyperintensities and White Matter Beta-Amyloid Deposition in Cognitively Unimpaired Elderly. Curr Alzheimer Res. Epub 2021 Mar 24.

41. Matías-Guiu JA, Cabrera-Martín MN, Matías-Guiu J, et al. Amyloid PET imaging in multiple sclerosis: an 18F-florbetaben study. BMC Neurol. 2015;15:243.

42. Pietroboni AM, Carandini T, Colombi A, et al. Amyloid PET as a marker of normal-appearing white matter early damage in multiple sclerosis: correlation with CSF β-amyloid levels and brain volumes. Eur J Nucl Med Mol Imaging. 2019;46:280–287.

43. Zhang M, Ni Y, Zhou Q, et al. 18F-florbetapir PET/MRI for quantitatively monitoring myelin loss and recovery in patients with multiple sclerosis: A longitudinal study. EClinicalMedicine. 2021;37:100982.

44. Glodzik L, Rusinek H, Li J, et al. Reduced retention of Pittsburgh compound B in white matter lesions. Eur J Nucl Med Mol Imaging. 2015;42:97–102.

45. de Paula Faria D, Copray S, Sijbesma JWA, et al. PET imaging of focal demyelination and remyelination in a rat model of multiple sclerosis: comparison of [11C]MeDAS, [11C]CIC and [11C]PIB. Eur J Nucl Med Mol Imaging. 2014;41:995–1003.

46. Maillard P, Mitchell GF, Himali JJ, et al. Aortic Stiffness, Increased White Matter Free Water, and Altered Microstructural Integrity: A Continuum of Injury. Stroke. 2017;48:1567–1573.

47. Pasternak O, Westin C-F, Bouix S, et al. Excessive Extracellular Volume Reveals a Neurodegenerative Pattern in Schizophrenia Onset. Journal of Neuroscience. 2012;32:17365–17372.

48. Pasternak O, Kubicki M, Shenton ME. In vivo imaging of neuroinflammation in schizophrenia. Schizophrenia Research. 2016;173:200–212.

49. Debette S, Beiser A, DeCarli C, et al. Association of MRI Markers of Vascular Brain Injury With Incident Stroke, Mild Cognitive Impairment, Dementia, and Mortality: The Framingham Offspring Study. Stroke. 2010;41:600–606.

50. Ibaraki M, Shimosegawa E, Toyoshima H, et al. Effect of Regional Tracer Delay on CBF in Healthy Subjects Measured with Dynamic Susceptibility Contrast-Enhanced MRI: Comparison with 15O-PET. Magnetic Resonance in Medical Sciences. 2005;4:8.

51. Ottoy J, Verhaeghe J, Niemantsverdriet E, Engelborghs S, Stroobants S, Staelens S. A simulation study on the impact of the blood flow-dependent component in [18F]AV45 SUVR in Alzheimer's disease. Gelovani JG, editor. PLoS ONE. 2017;12:e0189155.

52. Vipin A, Ng KK, Ji F, et al. Amyloid burden accelerates white matter degradation in cognitively normal elderly individuals. Hum Brain Mapp. 2019;40:2065–2075.

53. Baker SL, Harrison TM, Maass A, La Joie R, Jagust WJ. Effect of Off-Target Binding on ^{18}F-Flortaucipir Variability in Healthy Controls Across the Life Span. J Nucl Med. 2019;60:1444–1451.

54. Goubran M, Hammond RR, de Ribaupierre S, et al. Magnetic resonance imaging and histology correlation in the neocortex in temporal lobe epilepsy: MRI-Histology in Epilepsy. Ann Neurol. 2015;77:237–250.

55. Bodini B, Veronese M, García-Lorenzo D, et al. Dynamic Imaging of Individual Remyelination Profiles inMultiple Sclerosis. Ann Neurol. 2016;79:726–738.

56. Muñoz Maniega S, Meijboom R, Chappell FM, et al. Spatial Gradient of Microstructural Changes in Normal-Appearing White Matter in Tracts Affected by White Matter Hyperintensities in Older Age. Front Neurol. 2019;10:784.

57. Maillard P, Fletcher E, Lockhart SN, et al. White Matter Hyperintensities and their Penumbra Lie Along a Continuum of Injury In The Aging Brain. Stroke. 2014;45:1721–1726.

58. Reginold W, Sam K, Poublanc J, Fisher J, Crawley A, Mikulis DJ. Impact of white matter hyperintensities on surrounding white matter tracts. Neuroradiology. 2018;60:933–944.

Tables

Table 1. Demographics. Demographics within the low and high WMH groups. All values are indicated as mean ± standard deviation except for sex and Aß-positivity ($^{*}P<0.05$, $^{**}P<0.01$, $^{***}P<0.001$). Abbreviations: MMSE, mini-mental state examination; MoCA, Montreal cognitive assessment; WMH, white matter hyperintensity volumes.

Variables*	**Low WMH group (n = 57)**	**High WMH group (n = 58)**	*Test-statistic*
Age (years)	74.14 ± 5.58	76.90 ± 8.13	$t = -2.12^{*}$
Sex female, n (%)	34 (60)	26 (45)	$\chi^2 = 1.97$
Education (years)	16.02 ± 2.72	14.29 ± 2.59	$t = 3.48^{**}$
Composite [^{18}F]AV45 SUVR	0.98 ± 0.18	1.12 ± 0.23	$t = -3.59^{***}$
Total WMH (cm^3)	10.62 ± 12.93	34.65 ± 18.93	$t = -7.94^{***}$
BMI	27.51 ± 5.85	27.32 ± 5.23	$t = 0.18$
Hypertension, n (%)	28 (49%)	35 (60%)	$\chi^2 = 1.46$
Smoking, n (%)	32 (56%)	23 (40%)	$\chi^2 = 2.85$
MMSE	28.82 ± 1.45	27.10 ± 2.48	$t = 4.53^{***}$
MoCA	25.63 ± 2.53	22.57 ± 4.38	$t = 4.58^{***}$

[1] Hypertension was defined as systolic blood pressure ≥ 140 mmHg and/or diastolic blood pressure ≥ 90 mmHg.
* More extensive demographics are reported in Supplementary Table 2 of Ottoy et al. [28]

Figures

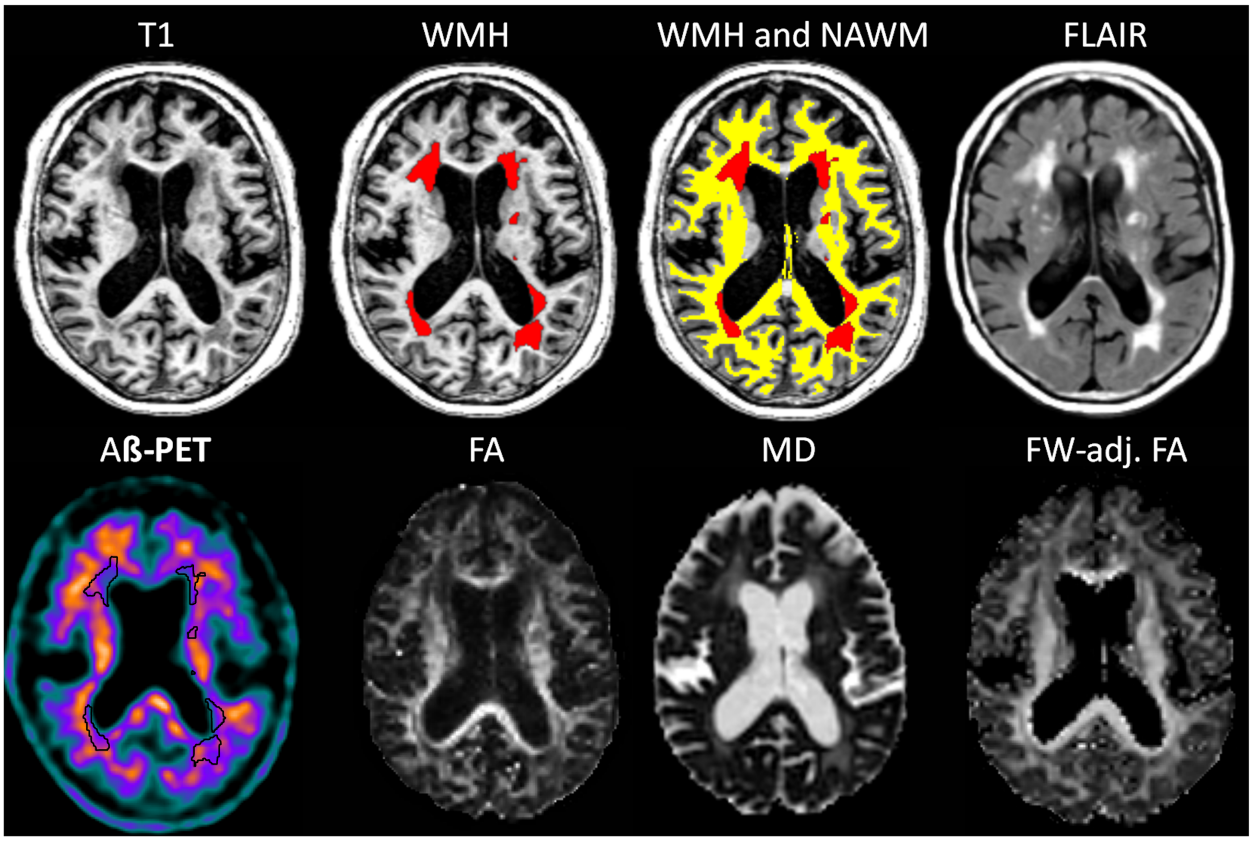

Figure 1. **Imaging acquisitions and segmentations in a representative subject**. (Upper panel, left to right:) T1-weighted scan, T1w image with WMH delineation (red), T1w image with delineation of both WMH (red) and NAWM (yellow), FLAIR image. (Lower panel, left to right:) 18F-AV45 PET, FA, MD, and FW-adjusted FA maps showing altered signal in the regions of WMH.

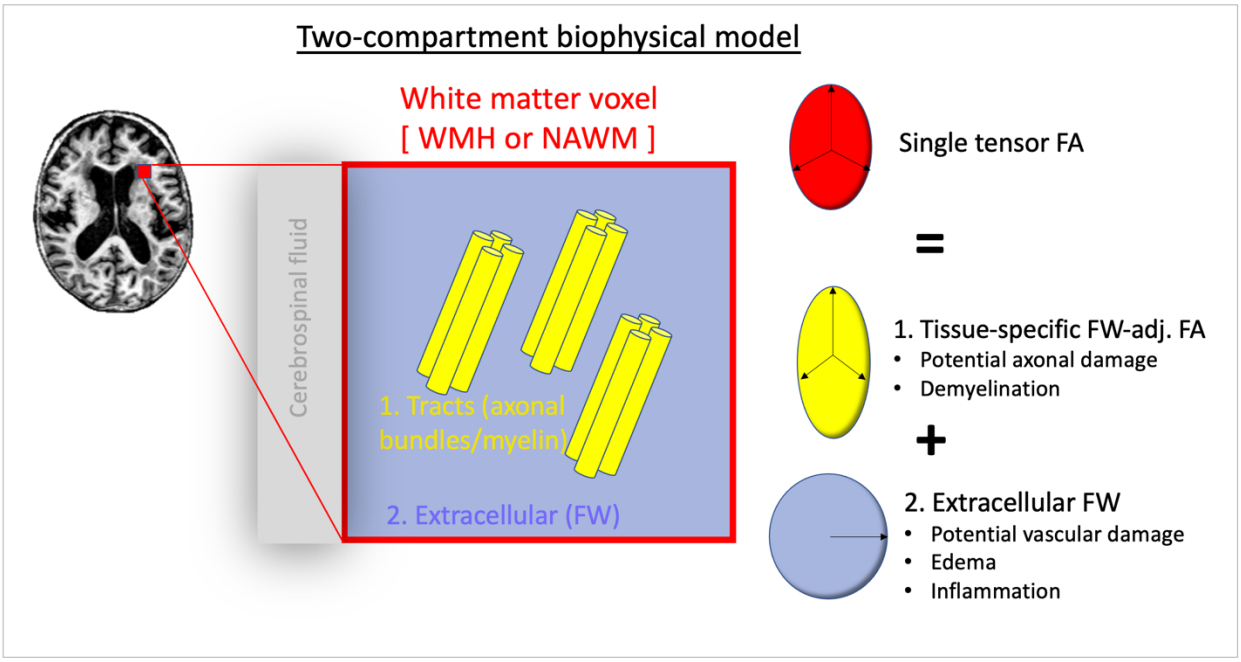

Figure 2. Schematic representation of the two-compartment biophysical DTI model. Each brain voxel (red color) of the NAWM or WMH can be separated into two compartments: an extracellular (FW; purple color) and a tissue-specific (FW-adjusted FA; yellow color) compartment. The 'adjusted' tissue diffusion ellipsoid is more prolate (yellow tensor) after being separated from the isotropic diffusion ellipsoid (purple tensor). Abbreviations: FA, fractional anisotropy; FW, free water; NAWM, normal-appearing white matter; WMH, white matter hyperintensities.

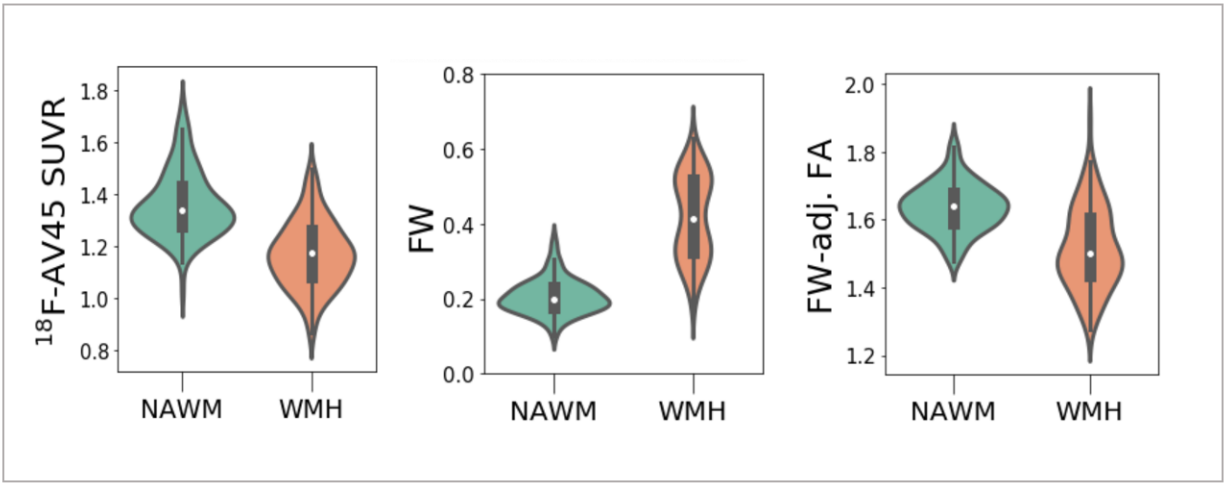

Figure 3. **Differences in ^{18}F-AV45 SUVR and DTI metrics between regions of WMH and NAWM**. Violin plots representing the group differences in ^{18}F-AV45 SUVR (left panel), FW (middle panel), and FW-adjusted FA (right panel) in the WMH (orange) vs. NAWM (green) across all subjects. Paired t-test showed significant differences between WMH and NAWM at $P<0.0001$ for all metrics. Specifically, ^{18}F-AV45 SUVR and FW-adjusted FA were significantly lower and FW higher in WMH compared to NAWM. Abbreviations: FA, fractional anisotropy; FW, free water; NAWM, normal appearing white matter; SUVR, standardized uptake value ratio; WMH, white matter hyperintensities.

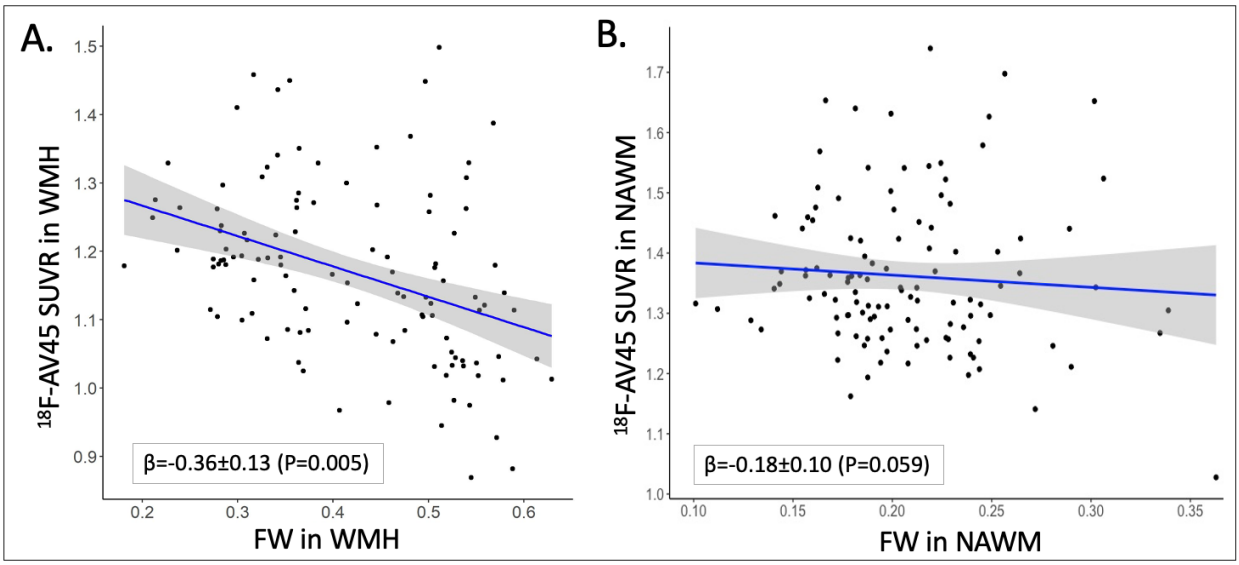

Figure 4. **Associations between FW and ^{18}F-AV45 SUVR.** Increased FW is associated with reduced ^{18}F-AV45 SUVR in WMH (panel A) but not in NAWM (panel B). Abbreviations: FW, free water; NAWM, normal appearing white matter; SUVR, standardized uptake value ratio; WMH, white matter hyperintensities.

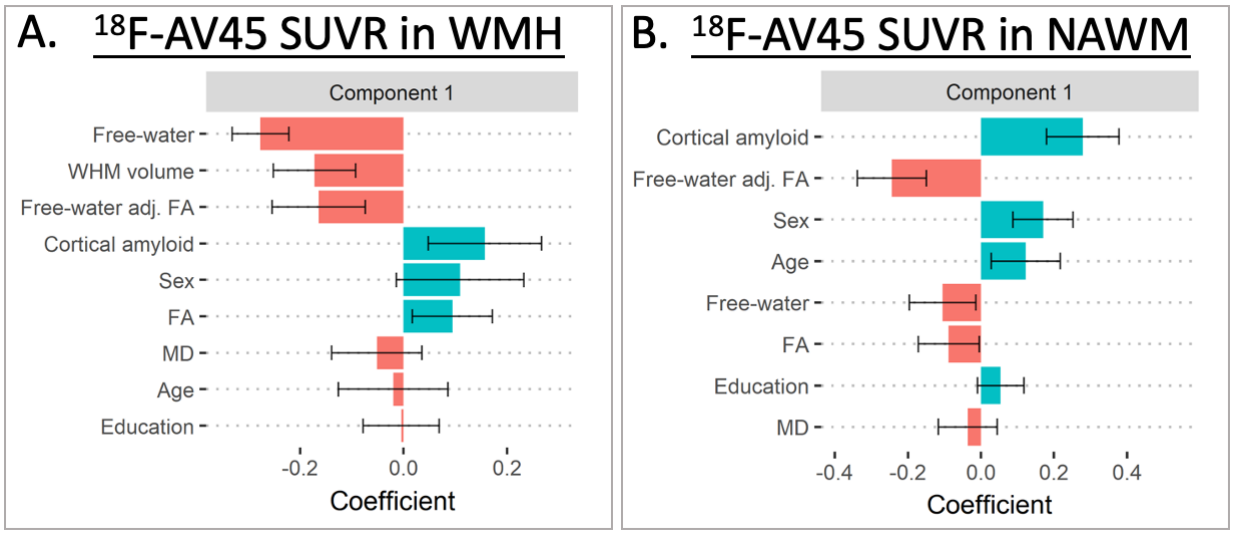

Figure 5. **PLS analysis showing how DTI metrics covary together in predicting ^{18}F-AV45 SUVR in regions of the WM.** The plots represent the contribution of the loadings to the first component of PLS analysis explaining most of the variance in ^{18}F-AV45 SUVR in WMH (panel A) and NAWM (panel B) in the high WMH group. Predictors include DTI metrics (FA, MD, FW, and FW-adjusted FA), demographics (age, sex, education), and imaging variables (WMH volume and cortical Aβ SUVR). Predictors are ordered based on the absolute value of the loading: FW and WMH volume had the most influence on ^{18}F-AV45 signal in the WMH while cortical Aβ and FW-adjusted FA had the most influence on ^{18}F-AV45 signal in the NAWM. Error bars represent 95%CI based on bootstrapping with 5,000 repetitions. Results with all subjects combined are represented in Supplementary Figure 2. Abbreviations: FW, free water; MD, mean diffusivity; NAWM, normal appearing white matter; SUVR, standardized uptake value ratio; WMH, white matter hyperintensities

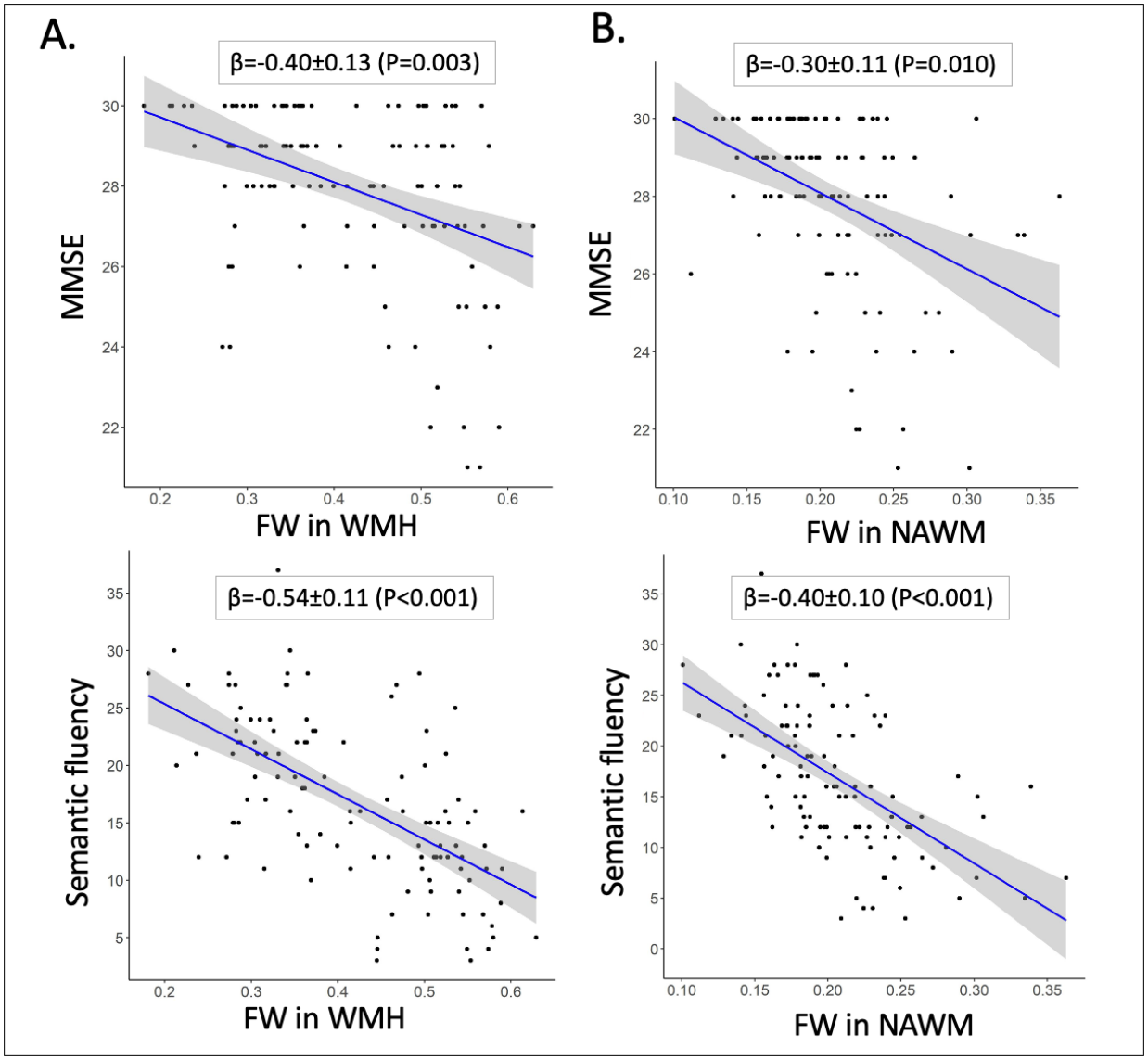

Figure 6. **Associations between FW and cognition.** Increased FW in the WMH (panel A) or NAWM (panel B) associate with cognitive impairment, including MMSE (upper row) and semantic fluency (lower row), across all subjects. Abbreviations: bs, bootstrap; FW, free water; MMSE, mini-mental state examination; NAWM, normal appearing white matter; WMH, white matter hyperintensities.